ρ_0 in Eq. (21) is the normalization factor, which can be expressed in terms of r_0 and a. For the muon mass, aluminum mass and the fine-structure constant we use the values $m_\mu = 105.6584$ MeV, $m_{\rm Al} = 25133$ MeV, $\alpha = \frac{1}{137.036}$, and remember that we take the electron to be massless. We numerically solve the radial Dirac equations for the muon and the electron, with the charge distribution in Eq. (21), to obtain the wavefunctions. For the muon energy, we obtain

$$E_\mu = m_\mu - E_b = 105.194 \text{ MeV}, \tag{23}$$

which gives the end-point energy

$$E_{\mu e} = E_\mu - \frac{E_\mu^2}{2m_{\rm Al}} = 104.973 \text{ MeV}. \tag{24}$$

Electron screening will increase the end-point energy in Eq. (24) by about +0.001 MeV and similarly shift the overall spectrum. That small effect is negligible for our considerations. Recall that the sum over K in Eq. (18) goes from 0 to ∞, we include as many terms in K as necessary in order to get three-digit precision for each point of the spectrum. This requires about 30 terms near $m_\mu/2$ and fewer terms in the low- and the high-energy parts of the spectrum.

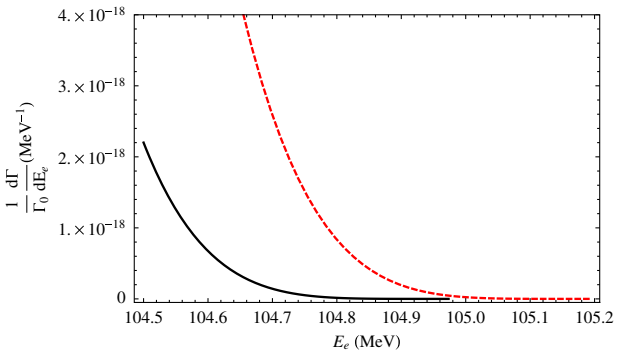

FIG. 2 (color online). Detail of the electron spectrum for aluminum very close to the high-energy end-point with (neglecting) nuclear-recoil, represented as the solid (dashed) line.

We present the result of the numerical evaluation of the high-energy region of the electron spectrum in Fig. 1. The squares in the figure are the spectrum with recoil effects, from Eq. (18). For comparison, we also show the result obtained by neglecting recoil effects, from Eq. (10), as the triangles. The right plot in the figure is a zoom for $E_e > 100$ MeV, the solid and dashed lines on this plot correspond to the Taylor expansions in Eqs. (19) and (20), respectively. Terms up to $K = 4$ were included in Fig. 1. Figure 2 presents a detail of the electron spectrum very close to the high-energy end-point in linear scale. We can appreciate in that figure how the spectra with (solid line) and without (dashed line) recoil effects tend to zero at the corresponding endpoints (the end-point without recoil is at $E_e = E_\mu$). To make our results easier to use, we mention that the polynomial

$$P(E_e) \equiv a_5\delta^5 + a_6\delta^6 + a_7\delta^7 + a_8\delta^8, \tag{25}$$

with

$$\begin{aligned} a_5 &= 8.6434 \times 10^{-17}, \quad a_6 = 1.16874 \times 10^{-17}, \\ a_7 &= -1.87828 \times 10^{-19}, \quad a_8 = 9.16327 \times 10^{-20}, \end{aligned} \tag{26}$$

the energies expressed in MeV, and

$$\delta = E_\mu - E_e - \frac{E_e^2}{2m_{\rm Al}}, \tag{27}$$

fits very well the result for the electron spectrum in aluminum normalized to the free decay rate (squares in Fig. 1) for all $E_e > 85$ MeV (i.e., the difference between Eq.(25) and the squares in Fig.1 is not larger than the uncertainties discussed in the next section). Note that, in order to obtain a better fit for the whole $E_e > 85$ MeV region, the value of a_5, in Eq. (25), was not constrained to be that of the leading coefficient of the Taylor expansion in Table I.

For completeness, we also show the spectrum for the full range of electron energies in Fig. 3 as the circles, from Eq. (10). Terms up to $K = 31$ were included in this plot. The total decay rate for muon decay-in-orbit in aluminum is obtained by integrating the spectrum in Fig. 3. The result we obtain is

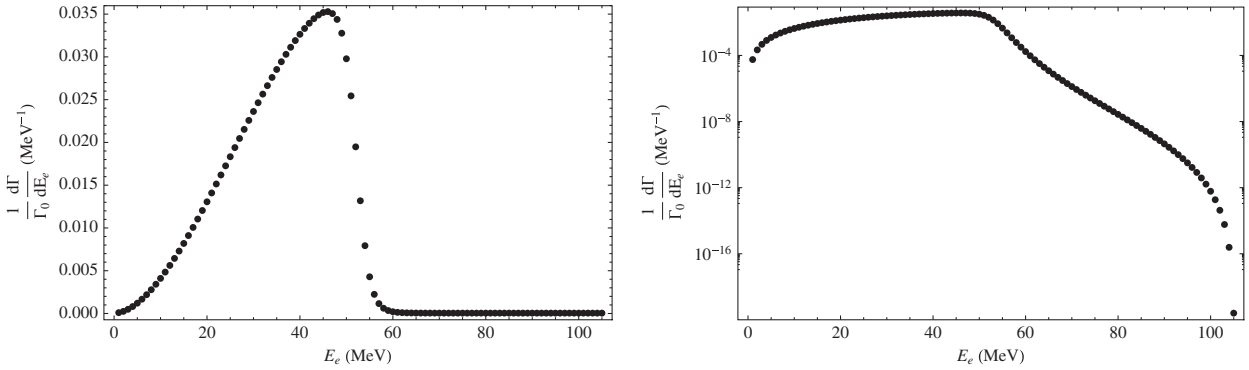

FIG. 3. Electron spectrum for aluminum. Left plot: linear scale; right plot: logarithmic scale.